Earthquakes produce carbon dioxide in crustal faults

Vincent Famin, Satoru Nakashima, Anne-Marie Boullier, Koichiro Fujimoto, Tetsuro Hirono

Earthquakes produce carbon dioxide in crustal faults

Vincent Famin[1], Satoru Nakashima[2], Anne-Marie Boullier[3], Koichiro Fujimoto[4] and Tetsuro Hirono[2]

[1]*Géosciences Réunion (LSTUR), Université de la Réunion, Institut de Physique du Globe de Paris / CNRS, UMR 7154. 15 avenue René Cassin, BP 7151. 97715 Saint Denis messag Cedex 9. La Réunion, France. Phone: +262 262 938 204. Fax: +262 262 938 266. E-mail: vfamin@univ-reunion.fr*

[2]*Osaka University, Graduate School of Science, Department of Earth and Space Science. 1-1 Machikaneyama-cho,Toyonaka-shi, Osaka 560-0043, Japan.*

[3]*Université Joseph Fourier, Laboratoire de Géophysique Interne et Tectonophysique / CNRS, Maison des Géosciences. BP 53X, 38041 Grenoble Cedex 9, France.*

[4]*Geological Survey of Japan, AIST-Earthquake Research Group, Tsukuba, Ibaraki, 305-8567 Japan.*

Fourier transform infrared (FTIR) micro-analysis of pseudotachylytes (i.e. friction-induced melts produced by seismic slip) from the Nojima fault (Japan) reveals that earthquakes almost instantaneously expel 99 wt% of the wall rock CO_2 content. Carbon is exsolved because it is supersaturated in the friction melts. By extrapolation to a crustal-scale fault rupture, large events such as the M7.2 Kobe earthquake (1995) may yield a total production of 1.8 to 3.4 $\times$ 10^3 tons CO_2 within a few seconds. This extraordinary release of CO_2 can cause a flash fluid pressure increase in the fault plane, and therefore enhance earthquake slip or trigger aftershocks; it may also explain the anomalous discharge of carbon monitored in nearby fault springs after large earthquakes. Because carbon saturation in silicate melts is pressure-dependent, FTIR can be used as a new tool to constrain the maximum depth of pseudotachylyte formation in exhumed faults.

Keywords: pseudotachylyte, infrared spectroscopy, fluids, CO_2 exsolution, earthquake, slip weakening, Nojima fault.

Introduction

An earthquake occurs because the shear resistance of a slipping fault becomes weaker with increasing slip [1]. The fault rocks are crushed by friction and may even melt if the heat generated is large enough [2]. Knowing how much energy is released as frictional heat, or converted into fractures and elastic waves, is essential for assessing how tectonic stress relaxation generates near-fault acceleration and surface damage, and how much stress is left

for future rupture of the Earth's crust. However, the production of heat is poorly constrained in the energy budget of earthquakes because the magnitude of fault weakening and its mechanism are not well known. In most theoretical or experimental mechanisms proposed to explain slip weakening, the lubricating agent is a fluid medium (either aqueous, melt or slurry) trapped within the fault plane and put under pressure by thermal or dynamic effects [3-8]. The efficiency of these slip-weakening mechanisms depends largely on the quantity of fluid involved and the pressurization achieved, which are difficult to assess. Therefore, determining the magnitude of coseismic shear stress reduction and the energy balance of earthquakes is still a major issue in seismology.

To constrain the fluid budget of a slipping fault and improve our understanding of weakening processes, we have analyzed the water and carbon dioxide content of pseudotachylytes (i.e. melts produced by friction during earthquakes) using a Fourier transform infrared microspectrometer (micro-FTIR). FTIR is a conventional tool for the study of volatile species in magmatic melts [9], albeit never applied to friction melts so far. We show that pseudotachylytes may be used to infer the fluid concentration in fault rocks at the time of seismic slip, providing new insights on earthquake mechanics.

The studied example is the Nojima fault (Fig. 1) that was activated on a dextral, 10.5 km-long surface rupture [10] by the Kobe (Hyogo-ken Nanbu) earthquake (M_{JMA} = 7.2, M_W = 6.9, focal depth = 16 km, January 17th, 1995), killing more than 6400 people. Immediately after the shake, the HCO_3^- concentration increased by 30 wt% in nearby springs [11]. This unexplained carbon discharge, together with other coseismic geochemical anomalies, decreased gradually to normal values in the following ten months [12-15]. One year after the earthquake, the Geological Survey of Japan drilled a borehole (Fig. 1) that reached the

upper boundary of the 83° dipping fault at 623.1 m depth within Cretaceous granodiorites [16]. The fault core consists in a 30 cm-thick cataclasite composed of quartz, albite and K-feldspar clasts derived from the granodiorite protolith, crushed together with secondary clays, zeolites and carbonates [16, 17]. The carbonates have a biogenic isotopic signature as well as present-day pore fluids in the fault, which suggests a superficial or sedimentary source for the alteration fluids in general and the carbon in particular [18-20]. Because of hydrothermal alteration, the cataclasite is enriched in SiO_2, CaO and depleted in MgO, Fe_2O_3, Na_2O, K_2O relative to the granodiorite protolith. The cataclasite also contains 3.5 to 10 wt% equivalent CO_2 with an average at 7.6 wt%, and 1 to 5 wt% H_2O with an average at 2.7 wt% (mean of 5 measurements taken from Figure 7 in [17]). This study focuses on two millimetre-thick pseudotachylytes (Fig. 2a) embedded in the cataclasite layers at 624.59 m within the Nojima fault core [17]. The texture of these pseudotachylytes has already been investigated in detail [21, 22] and is only summarized briefly. The dark layer of pseudotachylyte (PT1) contains fragments of cataclasite (isolated or aggregated quartz, albite and calcite clasts with molten rims) in a brown matrix. These fragments, and the fresh PT1 – cataclasite interface devoid of shear localization structures, indicate that the cataclasite is the precursory of PT1. A second, clearer pseudotachylyte (PT2), containing plastically deformed fragments of PT1 and fewer mineral remnants in a transparent matrix (Fig. 2a), re-melted the dark layer. The random occurrence of fluid-filled vesicles in the two matrixes, and the homogeneous aspect of these matrixes under the SEM [21] suggest that the two pseudotachylytes are made of undevitrified glass [22]. The composition of the vesicles (84 mol% H_2O; 15.3 mol% CO_2; 0.7 mol% NaCl) attest to the supersaturation of H_2O and CO_2 in the melts [22]. In addition, the molten rims of clasts in the two

pseudotachylytes indicate that melting reached a minimum temperature of 1200 °C [22], which is consistent with melting temperatures estimated from other pseudotachylyte samples in the Nojima fault [23]. The two matrixes have a dacite composition (~68 wt% SiO_2, 3 wt% Na_2O + K_2O) similar to the bulk composition of the cataclasite. Calcite fragments in the melts, and the fact that both matrixes contain up to twice the CaO content of the granodiorite protolith (4.06 wt%), imply that the precursory cataclasite was already carbonate-rich before melting. Carbonate precipitation continued between and after the melting events [24]. Pseudotachylytes were quenched at ambient temperatures of 150 – 350 °C and a depth range of 4 – 15 km [22, 25, 26]. These pseudotachylytes formed well after the cooling of the granodiorite basement (74 Ma [27]), and were then uplifted with the basement by a left-lateral thrust motion of the fault, mostly before the Eocene [26]. Exhumation is still occurring in the present even though the fault has shifted to a right-lateral thrust movement since the Plio-Pleistocene [28]. It is therefore likely that these exhumed pseudotachylytes represent slipping processes similar to those occurring today between the Kobe earthquake hypocenter and the surface. The multiple occurrence of pseudotachylytes within carbonate-bearing cataclasites on surface exposures of the Nojima fault [23], and on other faults along the Median Tectonic Line running through Japan, suggests that the lateral extent of melts is large, and/or that friction melting is a widespread phenomenon along those faults.

Analytical methods and results

Infrared spectra were measured on a JASCO, FTIR 620plus, IRT 30 apparatus, equipped with an automatic XY mapping stage moving the sample at 50 µm steps on X and Y under the microscope. Spectra were acquired by collecting 50 scans in the range 6000 – 700 cm^{-1} with a 4 cm^{-1} resolution and a 50 × 50 µm aperture. Every ten spectra during the mapping, the automatic stage moved to a position beyond the sample in order to take a background air spectrum. All the spectra were automatically corrected from background by the JASCO Spectra Manager software, and then corrected using the same linear baseline in the range 5000 – 1300 cm^{-1}. The thickness of the wafer was measured using a laser scanning confocal microscope (KEYENCE VK-8500) at the centre and corners of each of the mapped areas, and was found to be 63 ± 3 µm. Absorbance peaks were converted into volatile concentrations following the conventional procedure for SiO_2-rich melts [9], assuming a glass density of 2.7 $g.cm^{-3}$. The total error on concentration estimates is 5 to 10 % [9]. Concentration maps were built using the JASCO Spectra Manager software.

Four areas were analyzed by FTIR in the sample (Fig. 2). Each 50 × 50 µm pixel corresponds to an infrared spectrum, and hence to a couple of H_2O and CO_2 concentrations (typical FTIR spectra provided in Fig. 3). The measured concentrations include the fraction of H_2O and CO_2 dissolved in the glass and the fraction trapped in fluid inclusions. Water is observed entirely as molecular H_2O (no dissolved OH). The two pseudotachylytes display a similar water content of about 2 wt% H_2O (Fig. 2b), except in cracks. There is, however, an extremely sharp contrast of molecular CO_2 concentration between the dark older PT1 containing up to 5000 ppm CO_2, and the clear younger PT2 nearly devoid of CO_2 (Fig. 2c). The presence of water and carbon dioxide dissolved as molecular species, not as ionic

112 species, is typical of dacite type, silica-rich melts [29]. In addition, CO_3^{2-} is detected as
113 secondary carbonate minerals (mostly calcite) precipitated in microcracks or as mineral
114 fragments in the glass (Fig. 2d). PT1 contains 1 wt% CO_3^{2-} or 0.7 wt% equivalent CO_2
115 (average of all the spectra measured on PT1). Because PT2 is younger and less fractured
116 than PT1, it contains only 0.3 wt% CO_3^{2-} or 0.2 wt% equivalent CO_2 in average.
117 FTIR data are also reported in an H_2O-CO_2 diagram before (Fig. 4a) and after filtering (Fig.
118 4b) in order to consider only pure matrix glass without carbonates. PT1 contains 1.5 – 2.8
119 wt% H_2O and 1000 – 5000 ppm CO_2, whereas PT2 contains 1 – 2.8 wt% H_2O and 0 – 500
120 ppm CO_2 away from its contact with PT1.
121

122 Discussion and conclusion

123 1. Budget of volatile exsolution by friction melting

124 Our results show that friction melting causes carbon devolatilization of the fault rocks.
125 Because PT1 contains up to 0.7 wt% equivalent CO_2 as crystallized carbonates (i.e. 1 wt%
126 CO_3^{2-}, Fig. 2d), some carbonates may postdate the first melting event such that the
127 cataclasite possibly contained less carbon before PT1 formation than it does now, i.e. only
128 2.8 – 6.9 – 9.3 wt% equivalent CO_2 (minimum – average – maximum of Tanaka's et al.
129 measurements [17], minus 0.7 wt%). In order to set a lower bound to our quantification of
130 CO_2 loss, we therefore assume the precursory cataclasite to have contained no more than
131 2.5 – 3.5 wt% equivalent CO_2 before PT1. Even though, PT1 (1.5 – 2.8 wt% H_2O, 1000 –
132 5000 ppm CO_2) contains as much H_2O as the parent cataclasite, but about ten times less
133 CO_2. Likewise, PT2 (at 1 – 2.8 wt% H_2O, 0 – 500 ppm CO_2 away from its contact with

PT1) contains as much H_2O as PT1 from which it melted, but ten times less CO_2 (for a minimum estimate of the CO_2 loss, we neglect the carbonates precipitated after PT1 and before PT2). Therefore, each fusion expels at least 90 wt% of the CO_2 dissolved or trapped as carbonates in the protolith, because carbon is supersaturated in the molten phase. Only 1 wt% of the initial CO_2 content is kept in the fault plane after the two melting events, while the remaining 99 % are exsolved as fluid CO_2.

Assuming a rock density of 2.7 $g.cm^{-3}$, the fusion of 10^{-3} m^3 (i.e. 1 mm thickness $\times$ 1 m^2 of fault plane) of cataclasite (at 2.5 – 3.5 wt% CO_2) into PT1 (at 1000 – 5000 ppm CO_2) yields 56 to 95 g CO_2. Likewise, the re-fusion of 10^{-3} m^3 of PT1 into PT2 (at 0 – 500 ppm CO_2) releases 1.4 to 14 g CO_2 in 1 m^2 of fault plane. Frictional melting is therefore an unexpected and significant source of CO_2 in the Nojima fault.

2. Degassing behaviour of friction melts

FTIR data yield constraints on the ambient pressure during friction melting, because H_2O and CO_2 saturation in silicate melts is pressure-dependent. Spectra measured in PT1 define a trend in the high CO_2 field, whose slope indicates that the supersaturated melts were quenched while degassing an 80 mol% H_2O and 20 mol% CO_2 fluid mixture (Fig. 4b), consistent with the measured composition of fluid inclusions [22]. The lower end of the degassing trend (2 wt% H_2O, 1000 ppm CO_2) is the closer to the composition of the pure matrix glass without fluid inclusions. Considering the ~1200 °C temperature of melting, a maximum pressure of 300 MPa may then be estimated for the formation of the PT1 glass using the VolatileCalc software [30], or a 11 km depth assuming a 2.7 $g.cm^{-3}$ rock density.

156 Spectra acquired in PT2 lie in the low CO_2 range (Fig. 4b). The low slope of PT2 degassing
157 path suggests that the glass exsolved a much higher proportion of H_2O relative to CO_2 than
158 PT1 ($\geq$ 97 mol% H_2O, $\leq$ 3 mol% CO_2). If PT2 ever reached equilibrium saturation, it is
159 again in the lower end of the degassing path at less than 2 wt% H_2O and 200 ppm CO_2, or a
160 130 MPa maximum pressure (5 km). The consistency of these depths with independent
161 depth estimates [25, 26] implies that PT1 and PT2 nearly reached equilibrium volatile
162 saturation. Our results suggest that the two melting events occurred at different depths, and
163 therefore were separated by a large time span. FTIR mapping is a new method that provides
164 depth constraints on the formation of individual layers of glassy pseudotachylyte in
165 exhumed faults, without any assumption on the geotherm.
166 In addition, the solubility laws of volatiles in silicate melts may be used to explain the
167 degassing pattern during friction melting. In doing so, we assume that that H_2O and CO_2
168 exsolution in pseudotachylytes is ruled by local liquid-gas equilibrium as a first
169 approximation, keeping in mind that true equilibrium was probably not achieved within the
170 short time lapse of heating and quenching. Under this assumption, CO_2 exsolves faster than
171 H_2O due to the low solubility of carbon compared to H_2O. Consequently, a silicate melt
172 degassing in an open system (i.e. the exsolved fluid mixture is removed from the melt)
173 follows a steep path in the H_2O-CO_2 space, because CO_2 is almost entirely lost before H_2O
174 supersaturation begins. On the other hand, a magma degassing in a closed system (in which
175 the exsolved fluid stays in contact with the melt) follows a gently sloping path in the H_2O-
176 CO_2 space, because the partial pressure of CO_2 gradually increases in the exsolved phase
177 and hampers further CO_2 degassing. Accordingly, FTIR data reveal that each
178 pseudotachylyte degassing proceeds in two stages: 1) Loss of 90 wt% CO_2 without

179 significant H_2O loss from the cataclasite to PT1, and from PT1 to PT2 (dashed arrows in
180 Fig. 4b). This degassing path is consistent with an open system that prevails as long as the
181 melt viscosity is low enough for CO_2-rich bubbles to escape the pseudotachylytes. Because
182 it is an open system, this stage is not recorded in H_2O – CO_2 concentrations, yet is
183 evidenced by comparing volatile concentrations before and after melting. 2) Loss of water-
184 rich mixtures (80 mol% H_2O, 20 mol% CO_2 for PT1; $\geq$ 97 mol% H_2O, $\leq$ 3 mol% CO_2 for
185 PT2) is consistent with melts degassing in closed system (solid lines in Fig. 4b). This
186 second stage of closed system degassing occurs because the viscosity of the cooling melts
187 becomes too large to let the bubbles escape, resulting in the entrapment of fluid inclusions.
188 To summarize, pseudotachylytes in the Nojima fault behave as open systems at the
189 beginning of flash friction melting, and then as closed systems during the last stage of melt
190 cooling.
191

192 **3. Implication for fault mechanics**

193 The first essential implication of our findings is that CO_2 degassing may increase the fluid
194 pressure (P) in the fault zone during and/or after an earthquake, depending on the rate of
195 exsolution, the permeability of the fault core, the carbonate content of the precursory fault
196 rocks and the depth considered. To estimate the fluid pressure increase solely caused by
197 frictional exsolution, we consider the effect of CO_2 emission at constant temperature (~200
198 °C at 5 km and ~400 °C at 11 km), and neglect elastohydrodynamic or thermal
199 pressurization [4, 6-8], keeping in mind that these effects may be considerable if combined
200 with exsolution. Moreover, the ~15 volume % increase caused by the transformation of

cataclasite into pseudotachylyte is neglected, although it may contribute to increasing the fluid pressure and reducing the shear stress on the fault plane. For the sake of simplicity, we also consider the porosity of the fault zone to be entirely filled with pure CO_2, even though other fluids such as H_2O may be dominant before an earthquake. This assumption does not yield significant error in the calculation because the compressibility factors and viscosities of H_2O and CO_2 are nearly equal in the supercritical state within the pressure and temperature ranges considered here. Accordingly, the fluid pressure increase (P_f/P_0) is computed from the equation of state (EOS) of pure CO_2:

$$P = \frac{mZRT}{M^{CO_2}\phi w}, \tag{1}$$

which yields

$$\frac{P_f}{P_0} = \frac{\phi_0 Z_f m_f}{\phi_f Z_0 m_0} \tag{2}$$

Parameter values, units and definitions are given in Table 1. The subscripts *0* and *f* refer to quantities before and after exsolution, respectively. R, T, ϕ and M^{CO2} denote the gas constant, the temperature, the porosity of the fault zone and the molar mass of CO_2, respectively. Z, the compressibility factor of pure CO_2, is calculated using the Saxena and Fei EOS [31]:

$$Z = (1-0.5917)\left(\frac{T^c}{T}\right)^2 + 0.09122\frac{T^c P}{TP^c} + \left[1.4164\times10^{-4}\left(\frac{T^c}{T}\right)^2 - 2.8349\times10^{-6}\ln\frac{T}{T^c}\right]\left(\frac{P}{P^c}\right)^2 \tag{3}$$

where P^c and T^c represent the pressure and temperature at the critical point of CO_2. m_0 and m_f are the masses of CO_2 present before and after friction melting in a volume of fault zone

equal to $1 \times 1 \times w\ m^3$. m_0 is calculated assuming hydrostatic pressure in equation (1). m_f is equal to $(m_0 + m_e)$, where m_e is the mass of CO_2 exsolved by a 1 mm thick pseudotachylyte. w is the maximum distance of coseismic CO_2 outflow in the direction perpendicular to the fault plane, taken as the half width of the pseudotachylyte (0.5 mm) plus twice the hydraulic diffusion length scale of CO_2 (L_f). L_f is given by $L_f = \sqrt{D_f \psi}$ [8], ψ being the characteristic timescale of frictional exsolution, set at 5 sec (the time lapse for glass melting and quenching does not exceed a few seconds [32]). D_f is the hydraulic diffusivity after exsolution, given by $D_f = k_f / \eta \beta_f$, where k_f denotes the final permeability of the fault zone, β_f its storage capacity, and η the P-T dependent viscosity of supercritical CO_2. β_f is computed from $\beta_f = \beta^b - \beta^s + \phi_f(\beta_f^{CO_2} - \beta^s)$, β^s being the compressibility of mineral grains, β^b the bulk rock compressibility, and $\beta_f^{CO_2} = -\frac{P_f}{Z_f}\left(\frac{\partial Z/P}{\partial P}\right)_f^{T=cte}$ the compressibility of supercritical CO_2.

To calculate the pressure-dependent permeability of the slipping fault (k_f), we use an empirical law (Fig. 5) derived from the available data at different effective pressures (P_{rock}-P):

$$k = 3 \times 10^{-17} e^{-6.14 \times 10^{-8}(P_{rock} - P)} \quad (4)$$

Note that permeability in the Nojima fault is at least two orders of magnitude larger than the permeability of some other crustal faults (at similar effective pressures) investigated so far [8, 33-36]. In absence of specific laws of pressure dependence for ϕ and β^b on the Nojima fault core, we are left to adapt to our case the empirical relations determined on the Median Tectonic Line [8]:

$$\phi = \varphi e^{-2.97\times10^{-8}(P_{rock}-P)} \quad (5)$$

$$\beta^b = 2.5\times10^{-10} e^{-1.38\times10^{-13}(P_{rock}-P)} \quad (6)$$

using φ = 0.03, which is the mean porosity measured on samples from the Nojima fault core at room pressure [37].

The fluid pressure increase (P_f/P_0) due to frictional exsolution is depicted in Figure 6. At 11 km depth, a flash release of 56 – 95 g CO_2 per m^2 of fault plane raises the pore fluid pressure of 78 to 90 % above the hydrostatic pressure, or an 80 – 100 MPa increase, even without considering thermal pressurization. At 5 km, the release of 1.4 – 14 g CO_2 raises the fluid pressure by 5 – 15 % above the hydrostatic pressure. Note that the magnitude of fluid pressure increase strongly depends on the permeability of the fault core (Fig. 6), as do other mechanisms of pore pressurization. For example, at 11 km depth the fluid pressure increases by 100 – 110 % if the permeability is ten times smaller than the selected permeability law (Fig. 5), and is still of 50 – 60 % if the permeability is ten times larger. Frictional CO_2 exsolution can therefore be a significant pressurization mechanism in fault zones, even at relatively high permeability, and even at hydrostatic starting fluid pressure. Slip-weakening by frictional exsolution should be taken into account when considering earthquake processes at slip velocities large enough to produce friction melts. In addition, the low velocity of seismic waves from the Kobe earthquake aftershocks suggests the presence of high pore fluid pressures in the fault zone after the main shock [38]. Since the coseismic exsolution of CO_2 may sustain such fluid pressurization, it could also enhance later ruptures and trigger aftershock sequences in the Nojima fault, in a same way than mantle CO_2 degassing triggers aftershock trees in thrust faults from Northern Italy [39].

4. Implication for fault degassing

The second major consequence of our findings is that co-seismic carbon discharge in near-fault springs might result from friction melting. The relative abundance of pseudotachylytes in carbonate-rich cataclasites on different cores and outcrops of the Nojima fault suggest that coseismic CO_2 loss might be the rule rather than an exception. In addition, core sample studies conclude that magnitude 6 – 7 earthquakes are responsible for the formation of millimetre thick pseudotachylytes [22]. In the following discussion, we assume that an earthquake such as the M7.2 1995 Kobe earthquake produces pseudotachylytes at least as wide as those observed in cores [22] and outcrops [23] of the Nojima fault. Under this assumption, the friction melts caused by a single earthquake at 11 km and 5 km along the fault plane should be similar to the pseudotachylytes (PT1 and PT2) caused by two separate slip events in the sample. To calculate the minimum CO_2 production of a Kobe-like earthquake, we hence consider a very idealistic model in which the rupture produces PT1 from 11 km to 8 km and PT2 from 8 km to 5 km. The production of CO_2 beneath 11 km and above 5 km is unknown and therefore not considered, even though it might be significant. Accordingly, a minimum range of 170 to 330 kg CO_2 is released per meter of fault trace, or a total emission of $1.8 – 3.4\ 10^3$ tons CO_2 for a 10.5 km surface rupture of the Nojima fault such as in the Kobe earthquake. Note that thermal decomposition of carbonates in cataclasites could also contribute to release carbon in the Nojima fault, and hence increase the proposed budget. However, a large part of this CO_2 likely re-precipitates as new carbonate minerals soon after the earthquake. Yet a fraction of CO_2 may be

286 evacuated through the ground waters that leach the fault. Indeed, an excess of ~20 tons
287 equivalent CO_2 was emitted by the Awaji Island springs within the ten months of the Kobe
288 earthquake [11, 14], i.e. about 1 wt% of the CO_2 possibly produced by friction melting. As
289 the carbon isotopic signature in past and present ground waters from the Nojima fault is
290 biogenic and not consistent with a deep degassing source [18, 19], the coseismic carbon
291 discharge in springs might well have come from frictional exsolution. This possibility
292 opens promising applications for soil and spring gas monitoring in active faults, such as in
293 the San Andreas fault that is also degassing biogenic carbon [40]. In the absence of a deep
294 contribution, post-seismic CO_2 discharge might be taken as an evidence of frictional
295 exsolution. The amount of CO_2 released should be proportional to the amount of heated
296 carbon-bearing fault rock, and to the heat generated by shear friction. In deep wells probing
297 those faults, measuring the CO_2 flux could therefore provide an additional tool to constrain
298 the frictional strength of the fault, and the physical processes that govern seismic slip.

299

300 **Acknowledgments**

301 I. Basile-Doelsch, M. Bouchon, L. Jolivet, L. Michon, F. Renard and J. Rice are thanked
302 for improving former versions of the manuscript. We are grateful to John G. Spray and an
303 anonymous reviewer for their detailed and constructive comments. This work was
304 supported by grants from the Conseil Régional de la Réunion, from the CNRS "3F"
305 proposal and from the French embassy in Tokyo. This IPGP contribution number 2298.

306

307 **References**

308 1 H. Kanamori and E. Brodsky, 2004. Physics of Earthquakes. Reports on Progress in Physics 67(8),
309 1429-1496.
310 2 J.G. Spray, 1995. Pseudotachylyte controversy: Fact or friction ? Geology 23(12), 1119-1122.
311 3 D. McKenzie and J.N. Brune, 1972. Melting on fault planes during large earthquakes. Geophysical
312 Journal of the Royal Astronomical Society 29, 65-78.
313 4 A.H. Lachenbruch, 1980. Frictional heating, fluid pressure and the resistance to fault motion. Journal of
314 Geophysical Research 85, 6249-6272.
315 5 H.J. Melosh, 1996. Dynamic weakening of faults by acoustic fluidization. Nature 397, 601-606.
316 6 E.E. Brodsky and H. Kanamori, 2001. Elastohydrodynamic lubrication of faults. Journal of Geophysical
317 Research 106(B8), 16357-16374.
318 7 D.J. Andrews, 2002. A fault constitutive relation accounting for thermal pressurization of pore fluid.
319 Journal of Geophysical Research 107(B12), doi:10.1029/2002JB001942.
320 8 C.A.J. Wibberley, 2005. Earthquake slip weakening and asperities explained by thermal pressurization.
321 Nature 436, 689-693.
322 9 P.D. Ihinger, R.L. Hervig and P.F. McMillan, 1994. Analytical methods for volatiles in glasses. Reviews
323 in Mineralogy and Geochemistry 30(1), 67-121.
324 10 Y. Awata, K. Mizuno, Y. Sugiyama, R. Imura, K. Shimokawa, K. Okumura and E. Tsukuda, 1996.
325 Surface fault ruptures on the northwest coast of Awaji island associated with the Hogyoken Nanbu
326 earthquake of 1995, Japan. Journal of the Seismological Society of Japan 49, 113-124.
327 11 T. Sato and M. Takahashi, 1997. Geochemical changes in anomalously discharged groundwater in Awaji
328 Island -after the 1995 Kobe earthquake-. Chikyukagaku 31, 89-98.
329 12 C.Y. King, N. Koizumi and Y. Kitagawa, 1995. Hydrogeochemical anomalies and the 1995 Kobe
330 earthquake. Science 269, 38-39.
331 13 U. Tsunogai and H. Wakita, 1995. Precursory chemical changes in ground water: Kobe earthquake,
332 Japan. Science 269, 61-62.
333 14 T. Sato, R. Sakai, K. Furuya and T. Kodama, 2000. Coseismic spring flow changes associated with the
334 1995 Kobe earthquake. Geophysical Research Letters 27(8), 1219-1222.
335 15 R. Sugisaki, T. Ito, K. Nagamine and I. Kawabe, 1996. Gas geochemical changes at mineral springs
336 associated with the 1995 southern Hyogo earthquake (M=7.2), Japan. Earth and Planetary Science
337 Letters 139, 239-249.
338 16 T. Ohtani, K. Fujimoto, H. Ito, H. Tanaka, N. Tomida and T. Higuchi, 2000. Fault rocks and past to
339 recent fluid characteristics from the borehole survey of the Nojima fault ruptured in the 1995 Kobe
340 earthquake, soutwest Japan. Journal of Geophysical Research 106(B7), 16161-16171.
341 17 H. Tanaka, K. Fujimoto, T. Ohtani and H. Ito, 2001. Structural and chemical characterization of shear
342 zones in the freshly activated Nojima fault, Awaji Island, southwest Japan. Journal of Geophysical
343 Research 106(B5), 8789-8810.
344 18 T. Arai, T. Okusawa and H. Tsukahara, 2001. Behavior of gases in the Nojima Fault Zone revealed from
345 the chemical composition and carbon isotope ratio of gases extracted from DPRI 1800 m drill core. The
346 Island Arc 10(3-4), 430-438.
347 19 A. Lin, N. Tanaka, S. Uda and M. Satish-Kumar, 2003. Repeated coseismic infiltration of meteoric and
348 seawater into deep fault zones: a case study of the Nojima fault zone, Japan. Chemical Geology 202(1-
349 2), 139-153.
350 20 A. Ueda, A. Kawabata, K. Fujimoto, H. Tanaka, N. Tomida, T. Ohtani and H. Ito, 1999. Isotopic study
351 of carbonates in Nojima fault cores, in: The international workshop on the Nojima fault core and
352 borehole data analysis, H. Ito, K. Fujimoto, H. Tanaka and D. Lockner, eds., pp. 127-132, Geological
353 Survey of Japan, Tsukuba.
354 21 K. Fujimoto, H. Tanaka, N. Tomida, T. Ohtani and H. Ito, 1999. Characterization of fault gouge from
355 GSJ Hirabayashi core samples and implications for the activity of the Nojima fault, in: The International

workshop on the Nojima Fault core and borehole data analysis, H. Ito, K. Fujimoto, H. Tanaka and D. Lockner, eds., pp. 103-109, Geological Survey of Japan, Tsukuba.

22 A.M. Boullier, T. Ohtani, K. Fujimoto and H. Ito, 2001. Fluid inclusions in pseudotachylites from the Nojima fault, Japan. Journal of Geophysical Research 106(B10), 21965-21977.

23 K. Otsuki, N. Monzawa and T. Nagase, 2003. Fluidization and melting of fault gouge during seismic slip: Identification in the Nojima fault zone and implications for focal earthquake mechanisms. Journal of Geophysical Research 108(B4), doi:10.1029/2001JB001711.

24 A.-M. Boullier, K. Fujimoto, T. Ohtani, G. Roman-Ross, E. Lewin, H. Ito, P. Pezard and B. Ildefonse, 2004. Textural evidence for recent co-seismic circulation of fluids in the Nojima fault zone, Awaji island, Japan. Tectonophysics 378(3-4), 165-181.

25 K. Fujimoto, H. Tanaka, T. Higuchi, N. Tomida, T. Ohtani and H. Ito, 2001. Alteration and mass transfer inferred from the Hirabayashi GSJ drill penetrating the Nojima Fault, Japan. Island Arc 10(3-4), 401.

26 A.M. Boullier, K. Fujimoto, H. Ito, T. Ohtani, N. Keulen, O. Fabbri, D. Amitrano, M. Dubois and P. Pezard, 2004. Structural evolution of the Nojima fault (Awaji Island, Japan) revisited from the GSJ drill hole at Hirabayashi. Earth, Planets and Space 56, 1233-1240.

27 M. Murakami and T. Tagami, 2004. Dating pseudotachylyte of the Nojima fault using the zircon fission-track method. Geophysical Research letters 31(L12604), doi:10.1029/2004GL020211.

28 A. Murata, K. Takemura, T. Miyata and A. Lin, 2001. Quaternary vertical offset and average slip rate of the Nojima Fault on Awaji Island, Japan. The Island Arc 10, 360-367.

29 P.D. Ihinger, Y.-G. Zhang and E.M. Stolper, 1999. The speciation of dissolved water in rhyolitic melt. Geochimica et Cosmochimica Acta 63(21), 3567-3578.

30 S. Newman and J.B. Lowenstern, 2002. VOLATILECALC: a silicate melt-H_2O-CO_2 solution model written in Visual Basic for Excel. Computers & Geosciences 28, 597-604.

31 S.K. Saxena and Y. Fei, 1987. Fluids at crustal pressures and temperatures. 1. Pure species. Contribution to Mineralogy and Petrology 95, 370-375.

32 M.T. Swanson, 1992. Fault structure, wear mechanisms and rupture processes in pseudotachylyte generation. Tectonophysics 204(3-4), 223-242.

33 D. Lockner, C.A. Morrow, S.G. Song, S. Tembe and T.F. Wong, 2005. Permeability of whole core samples of Chelungpu fault, Taiwan TCDP Scientific drillhole. Eos Transactions of the American Geophysical Union 86(52), T43D-04.

34 C.A. Morrow and D. Lockner, 2005. Some recent laboratory measurements of fault zone permeability. Eos Transactions of the American Geophysical Union 86(52), T42B-04.

35 C.A. Morrow and J. Byerlee, 1992. Permeability of core samples from Cajon scientific drill hole: Results from 2100 to 3500 m depth. Journal of Geophysical Research 97(B4), 5145-5151.

36 C.L. Chu, C.Y. Wang and W. Lin, 1981. Permeability and frictional properties of San Andreas fault gouges. Geophysical Research letters 8(6), 565-568.

37 F. Surma, Y. Géraud and P. Pezard, 2003. Porosity network of the Nojima fault zone in the Hirabayashi hole (Japan), in: European Geophysical Society 2003, Geophysical Research Abstracts 5, pp. 12946, Nice.

38 D. Zhao, H. Kanamori, H. Negishi and D. Wiens, 1996. Tomography of the Source Area of the 1995 Kobe Earthquake: Evidence for Fluids at the Hypocenter ? Science 274, 1891-1895.

39 S.A. Miller, C. Collettini, L. Chiaraluce, M. Cocco, M. Barchi and B.J.P. Kaus, 2004. Aftershocks driven by a high-pressure CO_2 source at depth. Nature 427, 724-727.

40 J.L. Lewicki and S.L. Brantley, 2000. CO_2 degassing along the San Andreas fault, Parkfield, California. Geophysical Research letters 27(1), 5-8.

41 D.E. Moore, D.A. Lockner, C.A. Morrow and H. Tanaka, 2001. Permeability and strength of core samples from drillholes at the southern end of the Nojima Fault, Japan. Eos Transactions of the American Geophysical Union 87(47), Abstract S41A 0580.

42 D. Lockner, H. Naka, H. Tanaka, H. Ito and R. Ikeda, 1999. Permeability and strength of core samples from the Nojima fault of the 1995 Kobe earthquake, in: International workshop on the Nojima fault core and borehole data analysis, H. Ito, K. Fujimoto, H. Tanaka and D. Lockner, eds., pp. 147-152, Tsukuba.

43 K. Mizoguchi, T. Hirose and T. Shimamoto, 2000. Permeability structure of Nojima fault: Analysis of Funaki outcrop in Hohundan Tsuna-gun, Hyogo Prefecture. Earth Monthly Extra 31, 58-65.

44 E.W. Lemmon, M.O. McLinden and D.G. Friend, 2005. Thermophysical Properties of Fluid Systems, in: NIST Chemistry WebBook, NIST Standard Reference Database Number 69, P.J. Linstrom and W.G. Mallard, eds., National Institute of Standards and Technology, Gaithersburg MD, 20899 (http://webbook.nist.gov), 2005.

Figure caption

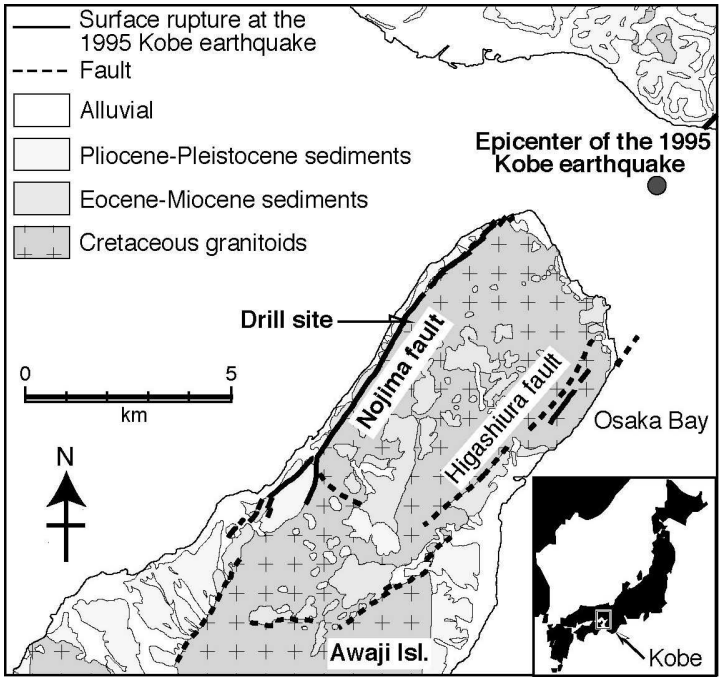

Figure 1: Simplified geological map of Awaji Island, modified from [16].

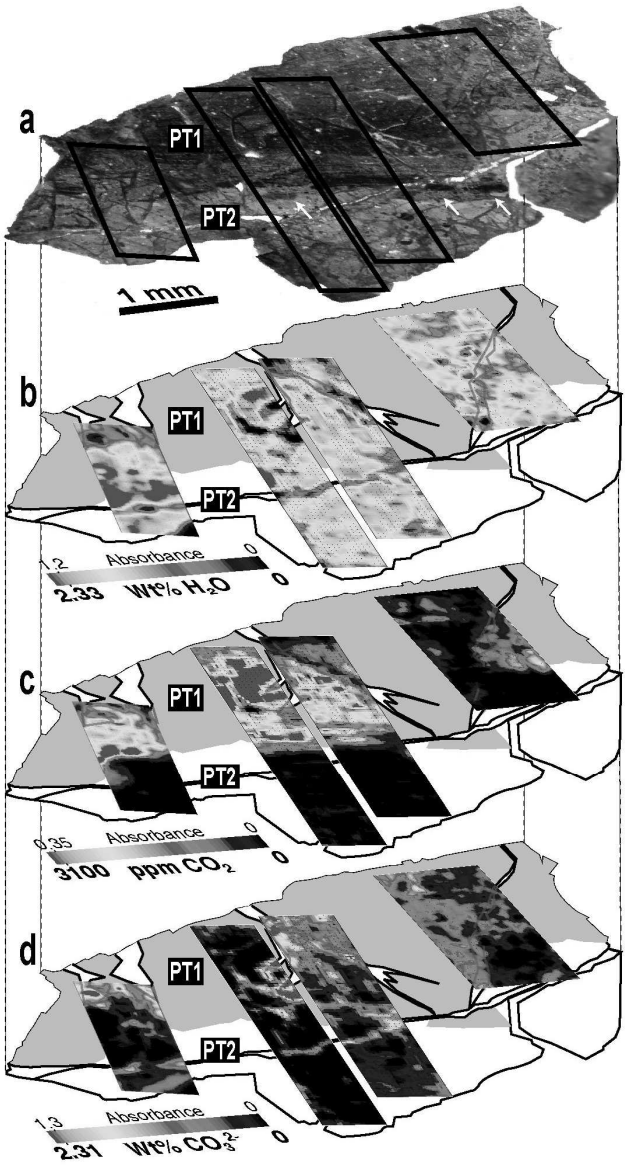

Figure 2: FTIR mapping in pseudotachylytes from the Nojima fault. a) Optical microphotograph showing the older dark pseudotachylyte (PT1) re-molten into a younger clear pseudotachylyte (PT2). PT2 contains plastically deformed fragments of PT1 (white arrows) and fewer mineral remnants than PT1. Carbonate veins crosscut the two generations of friction melts. b-d) Peak height (absorbance) mapping of molecular H_2O (1630 cm^{-1}), molecular CO_2 (2340 cm^{-1}) and CO_3^{2-} (1460 cm^{-1}) converted into concentrations (wt%).

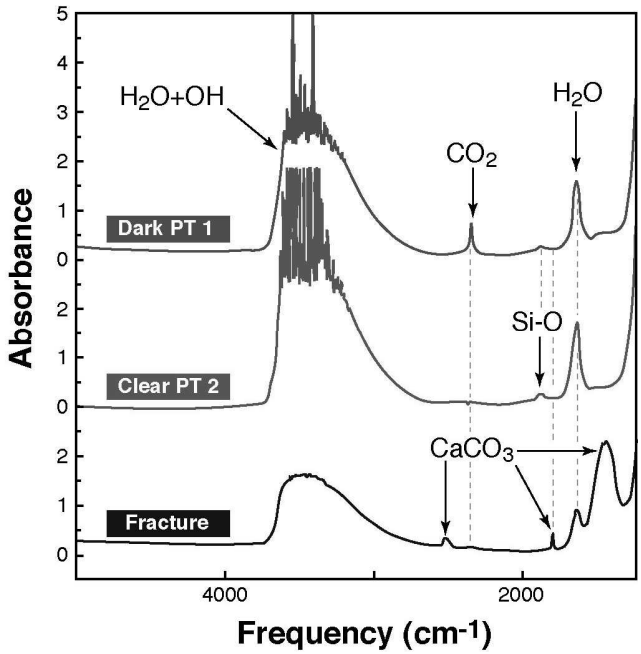

Figure 3: Typical FTIR spectra of pseudotachylytes from the sample cored in the Nojima fault. Upper (red) spectrum: dark older pseudotachylyte (PT1). Middle (green) spectrum: clear younger pseudotachylyte (PT2). Lower (blue) spectrum: fracture. There is virtually no dissolved hydroxyl in the glass (the absorption peak of bound OH is at 4500 cm^{-1}). The absorption peak of total OH (corresponding to the O-H stretching vibration at 3450 cm^{-1} in hydroxyl and water molecules) is saturated (and useless) in the glasses due to the high water concentration, but not in the fractured areas. The absorption peak of molecular CO_2 (recognized by its stretching vibration at 2340 cm^{-1}) is observed in the dark pseudotachylyte, but not in the clear one. Molecular H_2O (recognized by its bending vibration at 1630 cm^{-1}) displays a higher absorption peak and is therefore more abundant in the pure glass than in the fractures. The three absorption bands of calcite (at 2510, 1790 and 1460 cm^{-1}) are observed in fractured zones. A combination of Si-O vibrations (at 1870 cm^{-1}) is detected in pure glass.

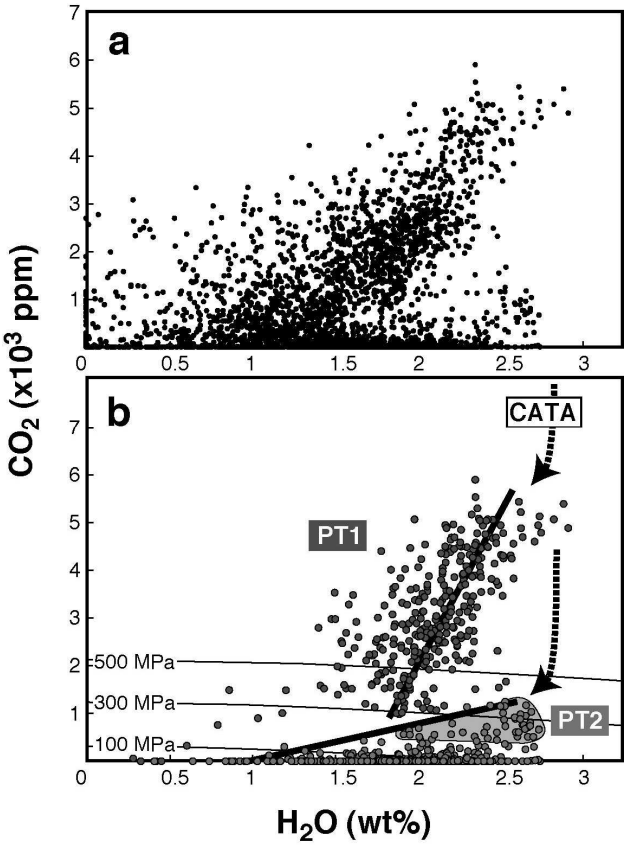

443

444 **Figure 4:** H_2O versus CO_2 concentrations measured by FTIR in the pseudotachylytes. a)
445 Complete dataset from the 3420 spectra. b) Dataset after filtering: spectra showing
446 carbonate peaks (2510, 1790 and 1460 cm^{-1}) were removed in order to consider only pure
447 glass without calcite. The isobars have been calculated using the VolatileCalc software
448 [30]. Pseudotachylytes first degas as an open system (thick dashed arrows). Because of
449 melt cooling, the pseudotachylytes eventually enter into a second step of closed-system
450 degassing (solid lines). The degassing trend of PT1 (red dots) is consistent with an exsolved
451 fluid phase at 80 mol% H_2O, 20 mol% CO_2 (upper solid line drawn by linear regression).
452 PT2 (green dots) degassed a more water-rich mixture ($\geq$ 97 mol% H_2O; $\leq$ 3 mol% CO_2,
453 domain delimited by the lower solid line). The shaded area corresponds to the border of
454 PT1, which is affected by incomplete re-melting and has a transitional CO_2 content between
455 fresh PT1 and final PT2 (Fig. 2c).

456

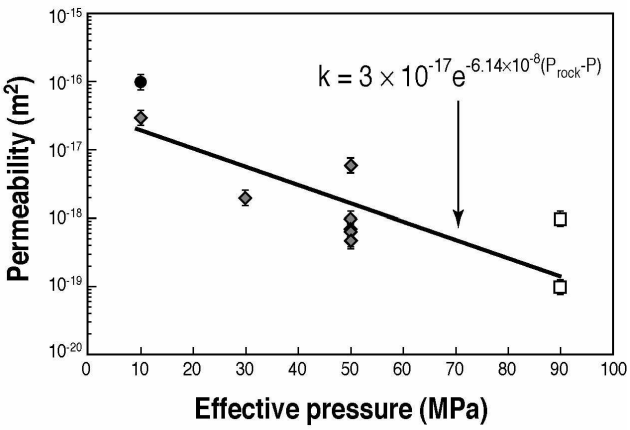

Figure 5: Best fit log-linear equation for permeability in the Nojima fault core with increasing effective pressure. Black dots compiled from [41], grey diamonds from [42], and empty squares from [43].

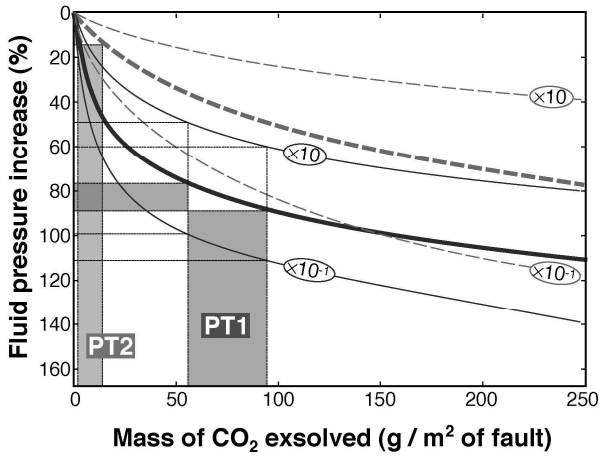

Figure 6: Fluid pressure increase (P_f/P_0) caused by CO_2 exsolution at two different depths, assuming a hydrostatic initial fluid pressure, and without considering thermal pressurization. Plain (blue) curves: 11 km, 400 °C. Dashed (orange) curves: 5 km, 200 °C. Each color set includes three curves: One curve calculated using the permeability law defined by equation 4 (Fig. 5), one curve using a permeability ten times larger (×10), and one curve using a permeability ten times smaller ($\times 10^{-1}$). The red and green areas correspond to the CO_2 production caused by PT1 (56 – 95 g/m^2) and PT2 (1.4 – 14 g/m^2), respectively, on 1 m^2 of fault plane. Calculation detailed in text.

471

472 **Table caption**

473 **Table 1:** Abbreviations and parameter values used in the calculation of the fluid pressure.
474

i	The subscripts i = 0 and i = f refer to quantities before and after CO_2 exsolution, respectively
P_i	Fluid pressure (Pa)
P_{rock}	Lithostatic load (Pa)
T	Temperature (K)
R	Gas constant = 8.314472 $J.mol^{-1}.K^{-1}$
Z_i	Compressibility factor of CO_2 given by the Saxena & Fei EOS [31]
T^c	Temperature of the critical point of CO_2 = 304.14 K [44]
P^c	Pressure of the critical point of $CO_2 = 73.8 \times 10^5$ Pa [44]
M^{CO2}	Molar mass of CO_2 = 44 $g.mol^{-1}$
m_i	Mass of fluid CO_2 in contained in a fault zone of thickness w, i.e. in the porosity of $1 \times 1 \times w$ m^3 of fault rock (g)
ϕ_i	Porosity of the fault zone
w	Maximum distance of CO_2 outflow in the direction perpendicular to the fault plane, within the time span of friction melting (m)
L_f	Hydraulic diffusion length scale of CO_2 (m)
D_f	Hydraulic diffusivity after exsolution ($m^2.s^{-1}$)
ψ	Characteristic timescale of frictional exsolution set at 5 sec (the time lapse for glass melting and quenching does not exceed a few seconds [32])
k_i	Permeability of the fault zone (m^2)
η_i	Viscosity (Pa.s) of CO_2 in the supercritical state (data from [44])
β_i	Storage capacity of the fault zone (Pa^{-1})
$\beta^{\square}_i$	Compressibility of the bulk fault core (Pa^{-1})
β^s	Compressibility of the mineral grains assumed to be constant at 1.2×10^{-11} Pa^{-1}
β_i^{CO2}	Compressibility of CO_2 (Pa^{-1})

475